

---

# X-RAY AND VISIBLE SPECTRA CIRCULAR MOTION IMAGES DATASET

---

A PREPRINT

**Mikhail O. Chekanov**

Institute for Information Transmission Problems  
(Kharkevich Institute)  
Moscow Institute of Physics and Technology  
(National Research University)  
chekanov@visillect.com

**Oleg S. Shipitko**

Institute for Information Transmission Problems  
(Kharkevich Institute)  
shipitko@visillect.com

October 2, 2019

## ABSTRACT

We present the collections of images of the same rotating plastic object made in X-ray and visible spectra. Both parts of the dataset contain 400 images. The images are made every 0.5 degrees of the object axial rotation. The collection of images is designed for evaluation of the performance of circular motion estimation algorithms as well as for the study of X-ray nature influence on the image analysis algorithms such as keypoints detection and description. The dataset is available at <https://github.com/Visillect/xvcm-dataset>.

**Keywords** circular motion estimation, camera circular motion, computed tomography, visual odometry, relative motion estimation, digital X-ray imaging

## 1 Introduction

Computed tomography is widely used in various fields: medicine [1], precise measurements [2], agriculture [3]. In tomography, the mutual trajectories of the sample, detector, and probe radiation source are usually considered known, since they are determined by the targeted movement of the setup components. Most of the computed tomography reconstruction methods rely on the geometric accuracy of the instrument and the reliably known trajectories of all its parts [4, 5]. However, the realized trajectory differs from the desired one for various reasons (mechanical backlash, an error in measuring the angle of rotation of an object, thermal deformations, the slope of the sample relative to the axis of rotation), which negatively affects the quality of the reconstruction. Thus, geometric errors are one of the main sources of reconstruction errors [6]. To compensate for these deviations different calibration approaches are used. These approaches can be divided into two classes. The first class of geometric calibration methods is based on observations of a specific object with a known geometry [7, 8, 9] or is based on reference measuring instruments [10, 11]. Geometric calibration is a laborious and expensive process, requiring the involvement of specialists with the appropriate qualifications. Moreover, geometrical errors inherent even in a calibrated system can still have a negative effect on the quality of reconstruction, and the quality of calibration decreases with time. The second class of methods called online calibration refines trajectory directly during measurements by analyzing obtained projections [12, 13, 14, 15, 16]. The online calibration methods do not require additional experiments and allow to compensate for geometric errors. Since circular motion estimation is of practical interest in tomography [6] we focus on this particular type of motion. While there are existing datasets for camera motion estimation with images in visible spectrum [17, 18, 19], there is no analogous dataset containing X-ray images. Moreover, the application of classical computer vision techniques to digital X-ray images requires an analysis of the influence introduced by the different nature of such images to the quality of algorithms. Again, here is no known dataset allowing to assess the influence of the translucent world model applicable for X-ray images on the algorithms developed for the classical opaque world model.

We present a dataset with digital X-ray images of a plastic object. The purpose of the presented dataset is twofold. It allows to measure the performance of circular motion estimation algorithms on X-ray images as well as to study the

difference in computer vision algorithms performance (e.g. keypoints detection and matching) while applied to visible and X-ray data.

## 2 Data description

The presented dataset consists of two parts: (i) images made in visible and (ii) X-ray spectra. The structure of the dataset is presented below:

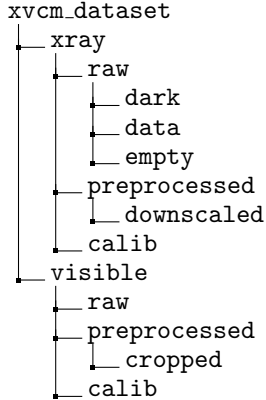


Figure 1 demonstrates samples images while Table 1 presents the dataset parameters. The X-ray part of the dataset was collected at the X-ray microtomograph developed and operating at the Federal Research Center for Crystallography and Photonics of Russian Academy of Sciences [20, 21] with the following parameters:

- exposure time – 5 seconds;
- radiation energy – 17 keV;
- monochromator – pyrographite;
- MoKa line.

While recording data the camera was stationary. The optical axis of the camera was perpendicular to the axis of object rotation. Such system setup is equivalent to the case of the circular camera motion around a stationary object (see Fig. 2).

### 2.1 Data preprocessing

To compensate for X-ray detector noise the following preprocessing algorithm was applied:

$$\text{preprocessed\_image}_{i,j} = \frac{\text{data}_{i,j} - \text{mean}(\text{dark}_{i,j})}{\text{mean}(\text{empty}_{i,j}) - \text{mean}(\text{dark}_{i,j})} \quad (1)$$

where  $i, j$  – pixel coordinates,  $\text{mean}()$  – is the mean value of pixels in the given coordinates over the whole subfolder, three subfolders contain the following images:

- dark – images taken in absence of X-ray radiation;
- empty – images taken in absence of object;
- data – images with rotating object.

Preprocessed images are stored in `xray\preprocessed`.

Due to the Canon EOS 5D Mark III camera limitations object of interest occupies only a small part of visible images. Folder `visible\preprocessed\cropped` contains cropped images of the size 407 x 407 pixels. To make visible and X-ray images comparable the latest were downscaled to the comparable resolution (407 x 360 pixels) in a aspect ratio preserving way (folder `visible\preprocessed\cropped`).

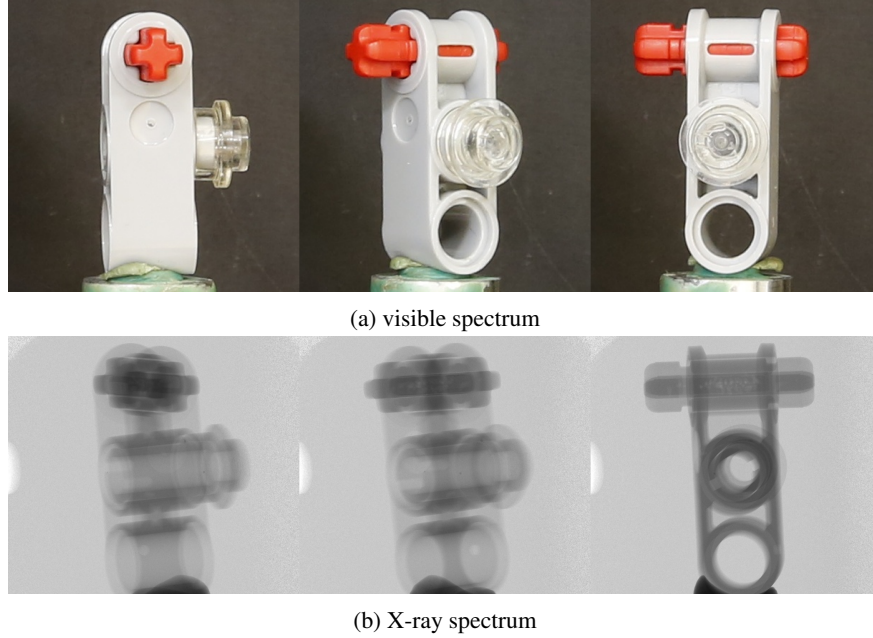


Figure 1: Examples of images presented in dataset for visible (a) and X-ray (b) spectrum.

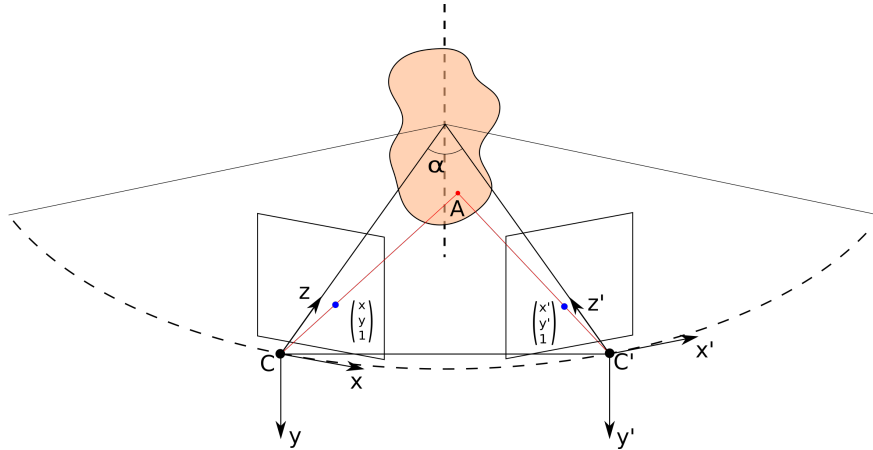


Figure 2: Circular camera motion.  $C$  and  $C'$  stand for camera centers in different moments of time,  $\alpha$  is a rotation angle,  $A$  is a point belonging to the observed object.

## 2.2 Calibration

Both parts of the dataset are accompanied by camera calibration parameters. In case of visible data, calibration was performed with the OpenCV toolbox [22] by detecting chessboard pattern. Calibration parameters as well as images used for calibration are stored in `visible\calib` folder. In the case of X-ray data calibration was obtained by the known dimensions of the object were used to estimate camera calibration parameters. The calibration is stored at `xray\calib`.

## 3 Conclusion

We presented the dataset containing both X-ray and visible images of the same rotating object. The presented dataset can be used while developing camera circular motion estimation techniques for online calibration methods. The second purpose of the presented dataset is the evaluation of the computer vision techniques applied to the X-ray data.

Table 1: Parameters of visible and X-ray dataset parts

Parameter	Visible	X-ray
Number of images	400	400
Rotation angle step	0.5°	0.5°
Resolution	5760 x 3840 pixels (object occupies an area of approximately 400 x 400 pixels)	3000 x 2650 pixels
Camera	Canon EOS 5D Mark III	Ximea xiRay11

## References

- [1] A Kesminiene and E Cardis. Cancer risk from paediatric computed tomography scanning: Implications for radiation protection in medicine. *Annals of the ICRP*, 47(3-4):113–114, 2018.
- [2] Andrea Buratti, Judith Bredemann, Michele Pavan, Robert Schmitt, and Simone Carmignato. Applications of ct for dimensional metrology. In *Industrial X-Ray Computed Tomography*, pages 333–369. Springer, 2018.
- [3] Stefan Mairhofer, Tony Pridmore, James Johnson, Darren M Wells, Malcolm J Bennett, Sacha J Mooney, and Craig J Sturrock. X-ray computed tomography of crop plant root systems grown in soil. *Current Protocols in Plant Biology*, 2(4):270–286, 2017.
- [4] Lee A Feldkamp, LC Davis, and James W Kress. Practical cone-beam algorithm. *Josa a*, 1(6):612–619, 1984.
- [5] Alexander Katsevich. An improved exact filtered backprojection algorithm for spiral computed tomography. *Advances in Applied Mathematics*, 32(4):681–697, 2004.
- [6] Massimiliano Ferrucci, Richard K Leach, Claudiu Giusca, Simone Carmignato, and Wim Dewulf. Towards geometrical calibration of x-ray computed tomography systems a review. *Measurement Science and Technology*, 26(9):092003, 2015.
- [7] Wim Dewulf, Kim Kiekens, Ye Tan, Frank Welkenhuyzen, and Jean-Pierre Kruth. Uncertainty determination and quantification for dimensional measurements with industrial computed tomography. *CIRP Annals*, 62(1):535–538, 2013.
- [8] Petr Hermanek, Massimiliano Ferrucci, Wim Dewulf, and Simone Carmignato. Optimized reference object for assessment of computed tomography instrument geometry. In *7th Conference on Industrial Computed Tomography*, pages 7–8, 2017.
- [9] Daniel Weiß, Ronald Lonardonì, Andreas Deffner, and Christoph Kuhn. Geometric image distortion in flat-panel x-ray detectors and its influence on the accuracy of ct-based dimensional measurements. In *iCT conference*, 2012.
- [10] Frank Welkenhuyzen, Bart Boeckmans, Ye Tan, Kim Kiekens, Wim Dewulf, and Jean-Pierre Kruth. Investigation of the kinematic system of a 450 kv ct scanner and its influence on dimensional ct metrology applications. In *Proceedings of the 5th International Conference on Industrial Computed Tomography*, pages 217–225, 2014.
- [11] Benjamin A Bircher, Felix Meli, Alain Küng, and Rudolf Thalmann. A geometry measurement system for a dimensional cone-beam ct. In *8th Conference on Industrial Computed Tomography, Wels, Austria (iCT 2018)*, 2018.
- [12] Kai Yang, Xinhua Li, X George Xu, and Bob Liu. Direct and fast measurement of ct beam filter profiles with simultaneous geometrical calibration. *Medical physics*, 44(1):57–70, 2017.
- [13] Yuan Xu, Shuai Yang, Jianhui Ma, Bin Li, Shuyu Wu, Hongliang Qi, and Linghong Zhou. Simultaneous calibration phantom commission and geometry calibration in cone beam ct. *Physics in Medicine & Biology*, 62(17):N375, 2017.
- [14] Feng Zhang, Jianping Du, Hua Jiang, Lei Li, Min Guan, and Bin Yan. Iterative geometric calibration in circular cone-beam computed tomography. *Optik-International Journal for Light and Electron Optics*, 125(11):2509–2514, 2014.
- [15] Jens Muders and Jürgen Hesser. Stable and robust geometric self-calibration for cone-beam ct using mutual information. *IEEE Transactions on Nuclear Science*, 61(1):202–217, 2014.

- 
- [16] Khanlian Chung, Lothar R Schad, and Frank G Zöllner. Tomosynthesis implementation with adaptive on-line calibration on clinical c-arm systems. *International journal of computer assisted radiology and surgery*, 13(10):1481–1495, 2018.
  - [17] Tomáš Hodan, Pavel Haluza, Štěpán Obdržálek, Jiri Matas, Manolis Lourakis, and Xenophon Zabulis. T-less: An rgb-d dataset for 6d pose estimation of texture-less objects. In *2017 IEEE Winter Conference on Applications of Computer Vision (WACV)*, pages 880–888. IEEE, 2017.
  - [18] OVG Group et al. Multi-view and oxford colleges building reconstruction, 2009.
  - [19] Steven M Seitz, Brian Curless, James Diebel, Daniel Scharstein, and Richard Szeliski. A comparison and evaluation of multi-view stereo reconstruction algorithms. In *2006 IEEE Computer Society Conference on Computer Vision and Pattern Recognition (CVPR'06)*, volume 1, pages 519–528. IEEE, 2006.
  - [20] AV Buzmakov, VE Asadchikov, DA Zolotov, BS Roshchin, Yu M Dymshits, VA Shishkov, MV Chukalina, AS Ingacheva, DE Ichalova, Yu S Krivonosov, et al. Laboratory microtomographs: Design and data processing algorithms. *Crystallography Reports*, 63(6):1057–1061, 2018.
  - [21] AV Buzmakov, VE Asadchikov, DA Zolotov, MV Chukalina, AS Ingacheva, and YS Krivonosov. Laboratory x-ray microtomography: Ways of processing experimental data. *Bulletin of the Russian Academy of Sciences: Physics*, 83(2):146–149, 2019.
  - [22] Gary Bradski and Adrian Kaehler. Opencv. *Dr. Dobbs journal of software tools*, 3, 2000.